Applied Catalysis B: Environmental 168-169 (2015) 51–61

Contents lists available at ScienceDirect

Applied Catalysis B: Environmental

journal homepage: www.elsevier.com/locate/apcatb

Novel visible-light-driven CQDs/Bi_2WO_6 hybrid materials with enhanced photocatalytic activity toward organic pollutants degradation and mechanism insight

Jun Di, Jiexiang Xia*, Yuping Ge, Hongping Li, Haiyan Ji, Hui Xu, Qi Zhang, Huaming Li*, Mengna Li

School of Chemistry and Chemical Engineering, Institute for Energy Research, Jiangsu University, 301 Xuefu Road, Zhenjiang 212013, PR China

ARTICLE INFO

Article history:
Received 9 October 2014
Received in revised form
25 November 2014
Accepted 30 November 2014
Available online 3 December 2014

Keywords:
CQDs
Bi_2WO_6
Hybrid material
Photocatalytic
Visible light irradiation

ABSTRACT

Novel visible-light-driven carbon quantum dots (CQDs)/Bi_2WO_6 hybrid materials were synthesized via a facile hydrothermal method. Multiple techniques were applied to investigate the structures, morphologies, optical and electronic properties and photocatalytic performance of as-prepared samples. The nanostructured hybrid material was formed with CQDs attached on the surface of Bi_2WO_6 sphere-like structure. The photocatalytic activity of the CQDs/Bi_2WO_6 hybrid materials was evaluated sufficiently by using rhodamine B (RhB), colorless antibiotic agent ciprofloxacin (CIP), tetracycline hydrochloride (TC), and endocrine disrupting chemical bisphenol A (BPA), as target organic pollutants. The as-prepared CQDs/Bi_2WO_6 hybrid materials exhibited much higher photocatalytic activities than pure Bi_2WO_6, which showed a broad spectrum of photocatalytic degradation activity. The enhanced activities were attributed to the interfacial transfer of photogenerated electrons from Bi_2WO_6 to CQDs, leading to effective charge separation of Bi_2WO_6. The modification by using CQDs (electron acceptor) was an effective way to improve photocatalytic efficiency, which can be extended to a general strategy for other semiconductors. The ESR analysis and free radicals trapping experiments indicated that the $O_2^{\bullet-}$ and h^+ were the main active species for the photocatalytic degradation. A possible mechanism of CQDs for the enhancement of visible light performance was proposed.

1. Introduction

Semiconductor-based photocatalysis has attracted massive attention due to its wide application in removing environmental pollutants and hydrogen production from splitting water using solar energy [1–3]. To effectively harness abundant natural sunlight, many visible-light-driven photocatalysts such as $BiVO_4$ [4], g-C_3N_4 [5], BiOX (X = Br, I) [6,7], Ag_3PO_4 [8] etc. have been successfully developed.

As one of the simplest Aurivillius oxides, bismuth tungstate (Bi_2WO_6) has aroused much attention due to its high stability, nontoxicity, suitable band gaps, and good photocatalytic activity [9,10]. Up to now, different methods such as solid state reaction [11], sol–gel [12], hydro/solvo-thermal method [13–15] etc. have been explored to prepare Bi_2WO_6 materials and various micro/nanostructures have been controllable synthesized [15–18]. However, the photocatalytic activity of pure Bi_2WO_6 is limited by its low efficiency of light absorption, difficult migration and high recombination probability of photo-generated electron–hole pairs. In order to improve the photocatalytic performance of Bi_2WO_6, numerous modification strategies have been used. Firstly, the chemical doping is an effective approach for changing the surface properties, extending the light responsive range and adjusting the electronic structure of semiconductors. Various metal and nonmetal dopants [19–24] have been used to improve the photocatalytic activity efficiently. In addition, the co-catalyst or sensitizer modification is another method to enhance the photocatalytic activity, using materials such as GO/RGO [25–27], C_{60} [28], and CuPc [29]. The co-catalyst can be acting as reaction sites, and accelerating the interfacial charge transfer from the semiconductor matrix to it. Besides, many different semiconductor materials [30–42] have been employed to couple with Bi_2WO_6 via the formation of heterojunction structure to improve the photocatalytic activity. Such heterojunction photocatalysts combine the synergistic effects of the individual materials [43]. However, the contact interfaces of these hybrid systems are insufficient and incompact, due to the large-size materials cannot

* Corresponding authors. Tel.: +86 511 88791108; fax: +86 511 88791108.
E-mail addresses: xjx@ujs.edu.cn (J. Xia), lhm@ujs.edu.cn (H. Li).

http://dx.doi.org/10.1016/j.apcatb.2014.11.057
0926-3373/

construct perfect interfaces. Thus, the surface defects will emerge through the formation of interfaces in the hybrid structures, and the electron–hole pairs will tend to recombine on surface defects and then limit the photocatalytic performance. In order to overcome this limitation, small-sized quantum dots materials can be used due to the uniform distribution and the formation of sufficient contraction. What is more, if the quantum dots materials possess excellent ability for charge transport, it could further construct the bulk-to-surface channels for the electrons. Thus, the architecture design of such a semiconductor-conductively quantum dots is worth of expectation.

Carbon quantum dots (CQDs), a new class of carbon nanomaterials with sizes below 10 nm, are typically quasi-spherical nanoparticles comprising amorphous to nanocrystalline cores with predominantly graphitic carbon (sp^2 carbon) or graphene and graphene oxide sheets fused by diamond-like sp^3 hybridized carbon insertions [44]. CQDs have gradually become a rising star, due to its robust chemical inertness, easy functionalization, high resistance to photobleaching, low toxicity and good biocompatibility [45–47]. It has been applied in a series of exciting areas, such as sensor [48,49], bioimaging [50,51], catalysis [52], photovoltaic devices [53,54] and so on. Due to the conjugated π structure of CQDs, it can exhibit the excellent electron transfer/reservoir properties. Very recently, CQDs have been introduced into semiconductors successfully, such as TiO_2 [55–57], Cu_2O [58], Fe_2O_3 [59,60], Ag_3PO_4 [61], ZnO [62], $BiVO_4$ [63], to improve the photocatalytic performance. However, the relationships between the structure and photocatalytic activity have not been systematic studied and the mechanism of pollutant photodegradation by CQDs based hybrid materials are still need to be further explored. Depending on the superiorities of Bi_2WO_6 and CQDs above mentioned, if the hybrid material of CQDs and Bi_2WO_6 is prepared, it is likely that this hybrid structure with higher photocatalytic performance can be obtained. To the best of our knowledge, there are no existing reports on the preparation and investigation of such a CQDs/Bi_2WO_6 system.

In this work, CQDs/Bi_2WO_6 hybrid materials have been first prepared via a facile hydrothermal route. The structures, morphologies, optical properties and photocatalytic properties are investigated in detail. The photocatalytic activities of CQDs/Bi_2WO_6 hybrid materials are evaluated sufficiently by the photocatalytic degradation of four different kinds of model pollutants. The relationships between the structure of the photocatalyst and the photocatalytic activities are also discussed in detail. The mechanism of pollutant photodegradation in this system is studied by using ESR analysis and free radicals trapping experiments.

2. Experimental

2.1. Synthesis of the photocatalysts

All the reagents were of analytical grade and were used without any further purification. The CQDs solid was synthetized according to the literature followed by the freeze-drying [64].

The CQDs/Bi_2WO_6 hybrid materials were synthesized via a facile hydrothermal process. In a typical procedure, 1 mmol $Na_2WO_4{\cdot}2H_2O$ was dissolved into 20 mL deionized water which contains a certain amount of CQDs. 2 mmol $Bi(NO_3)_3{\cdot}5H_2O$ was added into the above solution. The pH value of the solution was regulated to 1 by using nitric acid. After being stirred for 2 h, the suspension was added into 25 mL Teflon-lined autoclave. Then the autoclave was sealed in a stainless steel tank and heated at 140 °C for 24 h. Subsequently, the reactor was cooled down to room temperature naturally. The resulting samples were collected and washed with deionized water and ethanol and then dried at 50 °C in air for 24 h. The added contents of CQDs in the CQDs/Bi_2WO_6 hybrid materials were 1 wt%, 2 wt%, 4 wt%, respectively.

2.2. Characterization

A Shimadzu XRD-6000 X-ray diffractometer (Cu Kα source) was used to record X-ray powder diffraction (XRD) patterns with the 2θ range from 10° to 80° at a scan rate of 7°/min. X-ray photoelectron spectroscopy (XPS) measurement was performed on a VG MultiLab 2000 system with a monochromatic Mg-Kα source operated at 20 kV. FT-IR spectrum was performed on a Nicolet FT-IR spectrophotometer (Nexus 470, Thermo Electron Corporation) using KBr disks at room temperature. The scanning electron microscopy (SEM) measurements were carried out with a field-emission scanning electron microscope (JEOL JSM-7001F) equipped with an energy-dispersive X-ray spectroscope (EDS) operated at an acceleration voltage of 10 kV. Transmission electron microscopy (TEM) images were obtained from a JEOL JEM-2010 transmission electron microscope at an accelerating voltage of 200 kV. UV–vis diffuse reflection spectroscopy (DRS) was performed on a Shimadzu UV-2450 spectrophotometer using $BaSO_4$ as the reference. The nitrogen adsorption–desorption isotherms at 77 K were investigated using a TriStar II 3020 Surface Area and Porosity Analyzer (Micromeritics Instrument Corporation, USA). The PL spectra of the photocatalysts were detected using a Varian Cary Eclipse spectrometer. The photocurrent and electrochemical impedance spectroscopy (EIS) were measured by an electrochemical workstation (CHI 660B Chenhua Instrument Company). The electron spin resonance (ESR) signals of radicals spin-trapped by spin-trap reagent DMPO (Sigma Chemical Co.) in water were examined on a Bruker model ESR JES-FA200 spectrometer.

2.3. Photocatalytic experiments

The photocatalytic activities of the CQDs/Bi_2WO_6 hybrid materials samples were evaluated via the photocatalytic degradation of four different kinds of pollutants, such as rhodamine B (RhB), ciprofloxacin (CIP), bisphenol A (BPA) and tetracycline hydrochloride (TC) in aqueous solution under visible light irradiation. A 300 W Xe lamp with a 400 nm cutoff filter provided visible light irradiation. Aqueous solutions of RhB (100 mL, 10 mg L^{-1}), CIP (100 mL, 10 mg L^{-1}), BPA (100 mL, 10 mg L^{-1}) and TC (100 mL, 20 mg L^{-1}) were added in the different Pyrex photocatalytic reactors. In each experiment, 0.05 g of photocatalyst was added

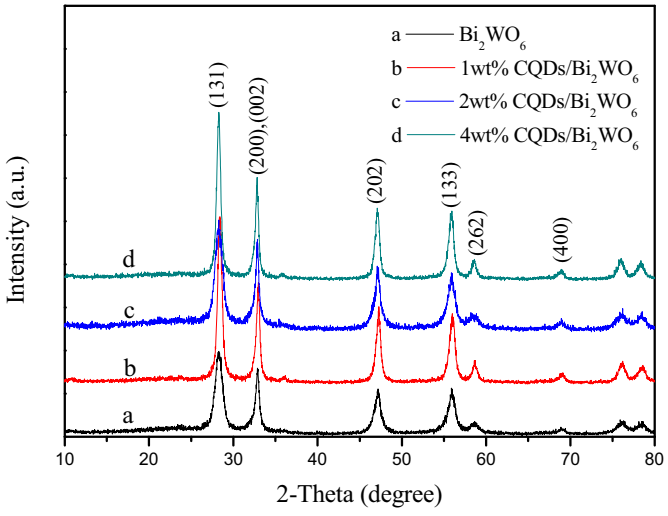

Fig. 1. XRD pattern of the as-prepared CQDs/Bi_2WO_6 hybrid materials.

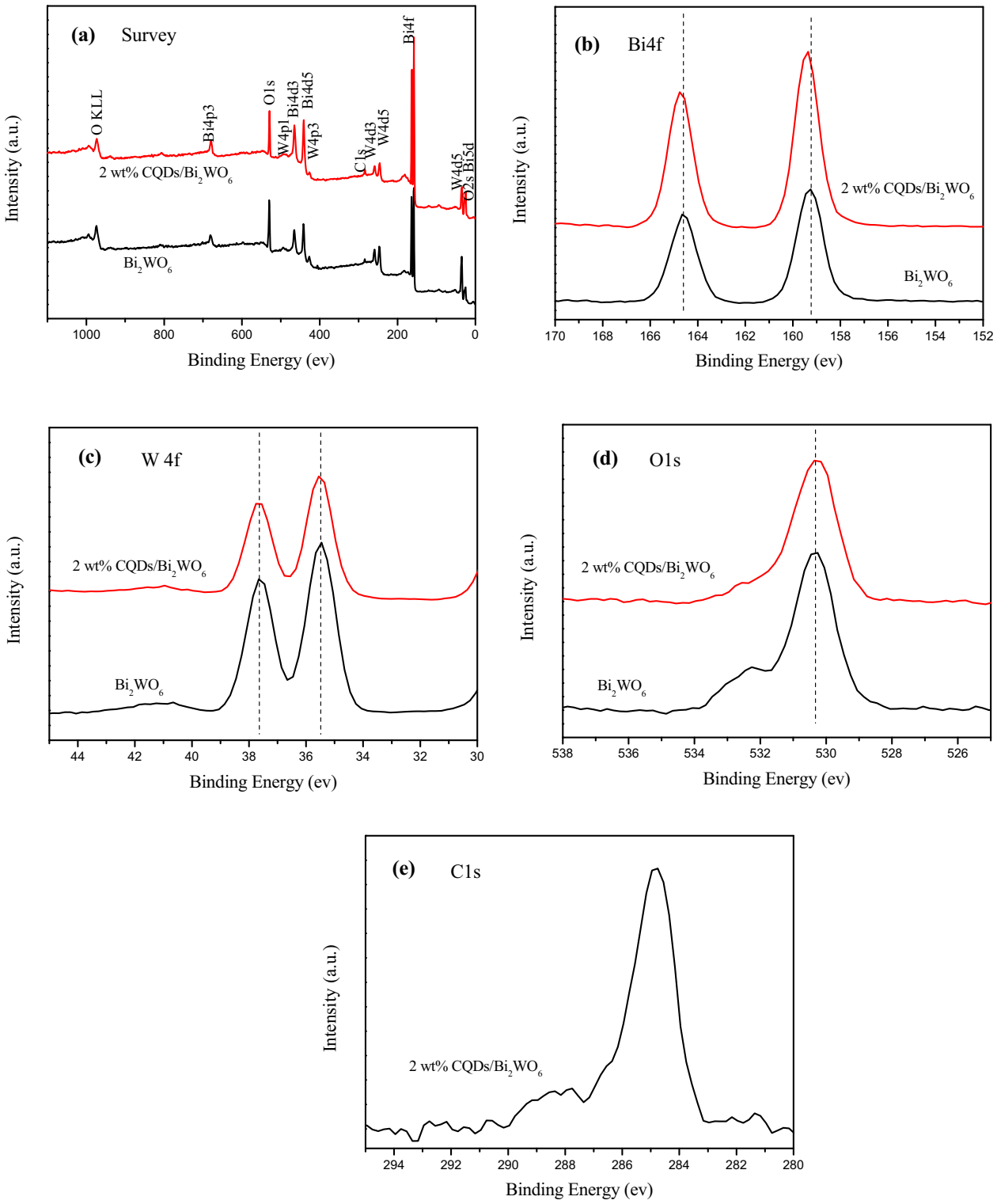

Fig. 2. XPS spectra of the pure Bi_2WO_6 and CQDs/Bi_2WO_6 hybrid materials. (a) Survey of the sample; (b) Bi 4f; (c) W 4f; (d) O 1s and (e) C 1s.

into the pollutant solution. Prior to irradiation, the suspensions were magnetically stirred in the dark for 30 min to achieve absorption–desorption equilibrium between the photocatalyst and pollutants. At certain time intervals, 3 mL suspensions were sampled and centrifuged (13,000 rpm, 3 min) to remove the photocatalyst particles. The concentrations of RhB, CIP, TC were monitored using an UV–vis spectrophotometer (UV-2450, Shimadzu) according to its absorbance at 553 nm, 276 nm, 356 nm, respectively. High performance liquid chromatography (HPLC) was applied to analyze the remnant amount of BPA. It was detected by two Varian ProStar 210 pumps, an Agilent TC-C18 column, and a Varian ProStar 325 UV-vis Detector at 230 nm. A solution of methanol and H_2O with the volume ratio 75:25 was used as the mobile phase at 1 mL min^{-1}, and 20 μL of the sample solution was injected. To investigate the active species generated in the photodegradation process, the experiments of free radicals ($^{\bullet}OH$, $O_2^{\bullet-}$ and h^+) capture were carried out by t-BuOH, BQ and EDTA-2Na (or AO), respectively.

2.4. Photoelectrochemical measurements

For the preparation of working electrodes, 2 mg of sample, 0.2 mL of ethanol and 0.2 mL of EG were mixed to produce a suspension and then 20 μL of the suspension was spread on a ITO glass electrode (0.5 cm × 1 cm). Electrochemical measurements were taken by using an electrochemical analyzer (CHI 660B Chenhua Instrument Company) in a standard three electrode system with a platinum plate as the counter electrode, and saturated Ag/AgCl electrode as the reference electrode. Phosphate buffered saline (0.1 mol L^{-1}, pH 7.0) was utilized as the electrolyte for the photocurrent measurement. The photosource was a 500 W Xe arc lamp. And the electrochemical impedance spectroscopy (EIS) measurement was performed in a 0.1 M KCl solution containing 5 mM $Fe(CN)_6^{3-}$/($Fe(CN)_6^{4-}$).

3. Results and discussion

3.1. Compositional and structural information

The composition and structure of pure Bi_2WO_6 and CQDs/Bi_2WO_6 hybrid materials with different CQDs contents are measured by XRD, XPS and FT-IR analysis. The phase structures of the as-prepared Bi_2WO_6 and CQDs/Bi_2WO_6 hybrid materials are examined by XRD (Fig. 1). The distinct diffraction peaks of samples can be found at 28.3°, 32.8°/32.9°, 47.1°, 56.0°, 58.5°, and 68.8°, which can be attributed to the (1 3 1), (2 0 0)/(0 0 2), (2 0 2), (1 3 3), (2 6 2), and (4 0 0) crystal planes of orthorhombic Bi_2WO_6 (JCPDS no. 39-0256), respectively. No other crystalline phase can be detected. Moreover, no signal about CQDs can be detected, which may due to the low CQDs content in the samples. The result can also be found in similar systems [61,63].

The surface chemical composition of Bi_2WO_6 and CQDs/Bi_2WO_6 samples, and the interaction between CQDs and Bi_2WO_6 is analyzed by XPS. The survey scan XPS spectrum (Fig. 2a) shows that the Bi_2WO_6 and CQDs/Bi_2WO_6 samples contain bismuth, tungsten, oxygen and carbon. For the Bi_2WO_6 sample, the spin–orbit components of Bi 4f peak are centered at approximate 159.2 eV and 164.6 eV (Fig. 2b), which corresponding to Bi^{3+} in crystal structure. The Bi 4f peak in the CQDs/Bi_2WO_6 sample displays a slight shift when compared to the Bi 4f peak in the Bi_2WO_6 sample. This indicates that the surface Bi chemical environment in the CQDs/Bi_2WO_6 has changed and can be referred to the presence of Bi–C interaction in the CQDs/Bi_2WO_6 sample [65]. The high-resolution W 4f XPS spectra of Bi_2WO_6 and CQDs/Bi_2WO_6 samples are shown in Fig. 2c. The binding energies of W 4f5/2 and W 4f7/2 are 37.6 eV and 35.5 eV in the oxide form of Bi_2WO_6, which can attributed to the W atoms existing in a 6+ oxidation state [30]. The O 1s peaks at 530.3 eV (Fig. 2d) can be assigned to the oxygen in Bi_2WO_6 crystals. Fig. 2e shows the high-resolution XPS spectra of C 1s. The main peak at 284.7 eV is ascribed to the C—C bond with sp^2 orbital. The XPS peaks of the C 1s centered at the binding energies of 286.5 eV and 288.4 eV are attributed to the C—O—C and C═O, respectively [59]. The result of XPS analysis reveals the coexistence of Bi_2WO_6 and CQDs in the CQDs/Bi_2WO_6 hybrid material.

FT-IR spectra are carried out to further determine the presence of CQDs in CQDs/Bi_2WO_6 hybrid materials. And the existing interactions between CQDs and Bi_2WO_6 can be further confirmed by FT-IR analysis. From Fig. 3, the stretching vibrations of OH at 3430 cm^{-1} and C—H at 2923 cm^{-1} and 2970 cm^{-1} can be observed. The absorption bands at 570 cm^{-1} and 1380 cm^{-1} are ascribed to Bi—O stretching mode and W—O—W bridging stretching modes, which imply the existence of Bi_2WO_6. For the CQDs/Bi_2WO_6 hybrid materials, the absorption peaks located at 1460 cm^{-1} appears, which could assigned to the absorption peaks of —COO^- and

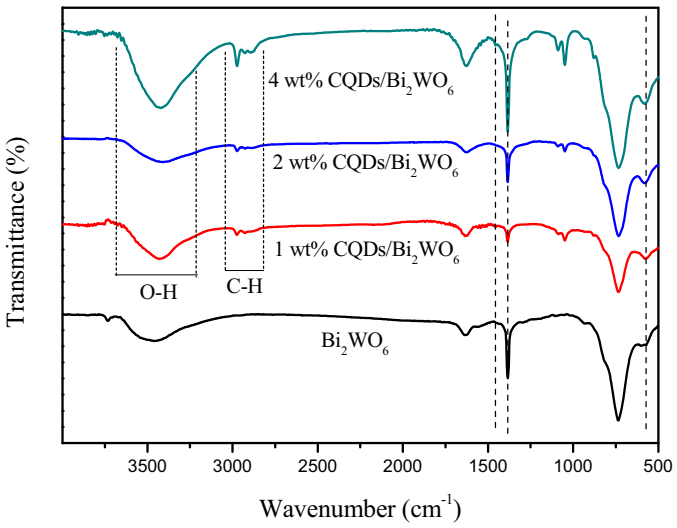

Fig. 3. FT-IR of CQDs/Bi_2WO_6 hybrid materials with different contents of CQDs.

thus reveal the existence of CQDs [66]. The characteristic peak of 570 cm^{-1} moves to higher wavenumber in the FT-IR spectrum of CQDs/Bi_2WO_6 hybrid materials, indicating that an interface interaction between CQDs and Bi_2WO_6 occurs. The result of FT-IR analysis is consistent with the XPS analysis.

3.2. Morphology and textural property

The morphology and microstructure of the CQDs/Bi_2WO_6 hybrid materials are characterized by SEM and TEM analysis. Fig. 4a and b shows the SEM micrographs of the as-prepared CQDs/Bi_2WO_6 hybrid materials samples. The products are sphere-like structure with the average diameter about 3 μm (Fig. 4a). The entire sphere-like hierarchical structures consist of numerous Bi_2WO_6 nanosheets (Fig. 4b). The EDS pattern (Fig. S1) shows the CQDs/Bi_2WO_6 sample contain C, O, W and Bi element. It proves that the sample prepared is CQDs/Bi_2WO_6 hybrid material.

TEM analysis is applied to further explore the microstructure of CQDs/Bi_2WO_6 hybrid material (Fig. 4c–f). The TEM images of pure Bi_2WO_6 are also provided for comparison. Fig. S2a and b shows the TEM images of pure Bi_2WO_6 that some nanosheets can be found from the edge of sphere-like structure. Meanwhile, the obvious contrast between the dark edge and the relatively bright center confirms their hollow nature. From Fig. S2b, the surface is smooth of pure Bi_2WO_6 nanosheets. Compared to the pure Bi_2WO_6, the CQDs/Bi_2WO_6 hybrid material has the similar sphere-like structure with hollow nature, which implies that the introduction of CQDs to Bi_2WO_6 did not change the main morphology (Fig. 4c). It can be seen from Fig. 4d and e that a large number of CQDs are evenly attached to the surface of Bi_2WO_6 nanosheets, which is a strong evidence for explaining the formation of CQDs/Bi_2WO_6 hybrid material. Fig. 4f shows the HRTEM image of CQDs/Bi_2WO_6 hybrid material. The lattice spacing of CQDs is determined to be 0.321 nm, which corresponding to the (0 0 2) crystal plane [61,63]. The lattice fringe spacing of some CQDs cannot be observed and this is due to that CQDs are quasi-spherical nanoparticles comprising amorphous to nanocrystalline cores [64]. At the same time, the lattice spacing around 0.273 nm can be found, which agree well with the crystallographic (2 0 0) spacing of Bi_2WO_6. The above results further demonstrate that the CQDs have modified on the Bi_2WO_6 to construct CQDs/Bi_2WO_6 hybrid materials.

N_2 adsorption–desorption isotherms (Fig. 5) of the as-obtained samples are conducted to determine the surface area of the

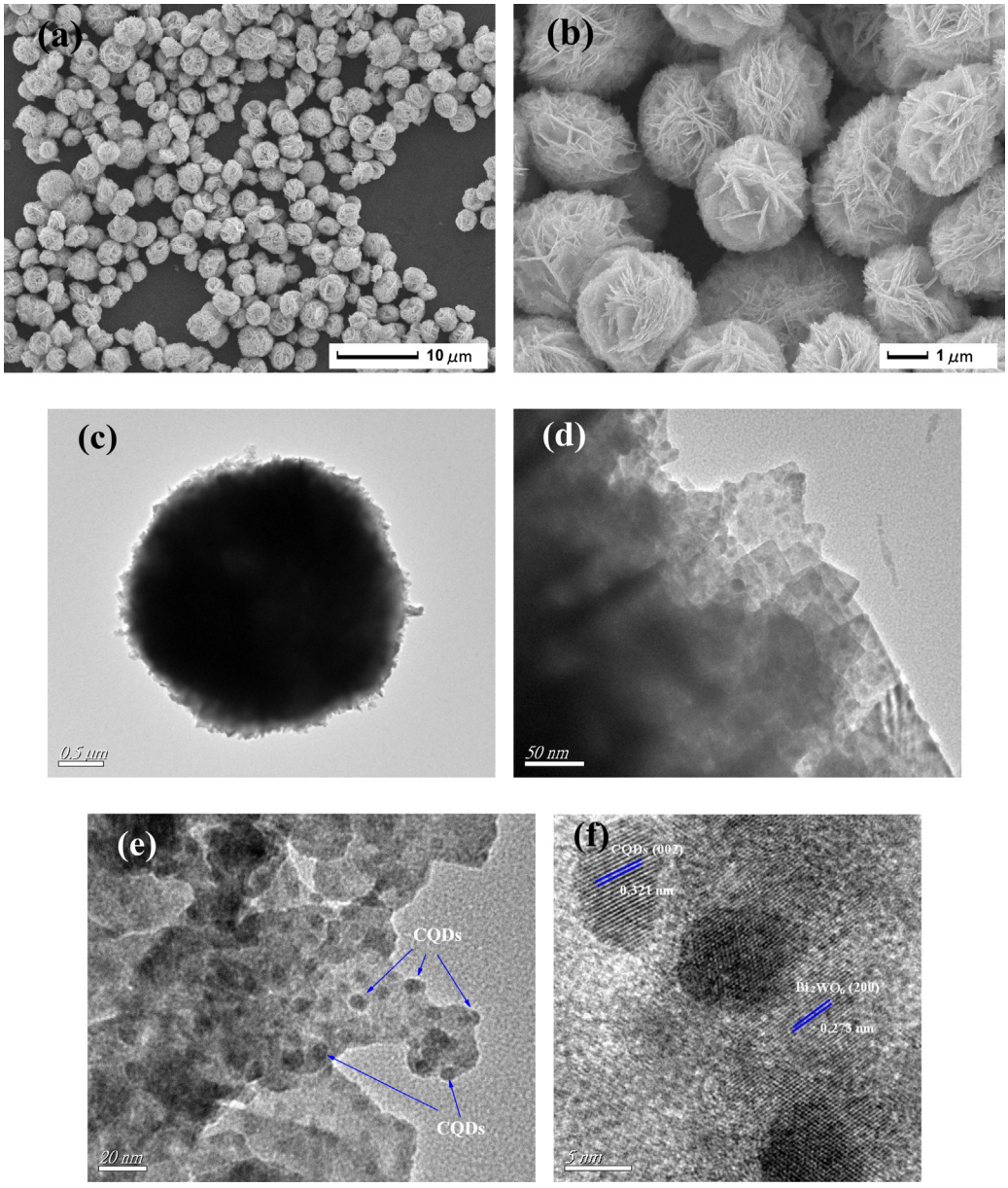

Fig. 4. SEM and TEM images of the 2 wt% CQDs/Bi_2WO_6 hybrid materials. (a) The low magnification SEM image; (b) high magnification SEM image; (c–e) low magnification TEM image and (f) high magnification TEM image.

hybrid materials. The specific surface area of the pure Bi_2WO_6, 1 wt% CQDs/Bi_2WO_6, 2 wt% CQDs/Bi_2WO_6 and 4 wt% CQDs/Bi_2WO_6 are calculated to be 37.17 $m^2\ g^{-1}$, 38.96 $m^2\ g^{-1}$, 48.20 $m^2\ g^{-1}$ and 53.96 $m^2\ g^{-1}$, respectively. It can be seen that the surface area improves as the introduction of CQDs to Bi_2WO_6. And the specific surface areas gradually increase when the mass ratio of CQDs increases from 1 wt% to 4 wt%. The improved specific surface areas are advantageous for absorb more active species and reactants on their surface, which thus favors the improvement of photocatalytic performance.

3.3. Optical and electronic properties

The light absorption property of pure Bi_2WO_6 and the CQDs/Bi_2WO_6 hybrid materials with different CQDs contents is analyzed via DRS, and the result is shown in Fig. 6. The pure Bi_2WO_6 exhibits the absorption in the region ranging from 200 nm to 450 nm. This absorption originates from the charge transfer response of Bi_2WO_6 from the valence band to the conduction band. For the CQDs/Bi_2WO_6 hybrid materials, the light harvesting capability within the visible light region enhanced with the increased CQDs contents. And the apparently red shift for CQDs/Bi_2WO_6 hybrid materials appears when compared with pure Bi_2WO_6. The enhanced light absorption may results in forming more electron–hole pairs and thus leads to an enhanced photocatalytic activity [67].

Photoluminescence (PL) spectra have been widely used to reveal the charge transfer, migration and recombination processes in photocatalysts. As is known, weaker intensity represents lower recombination probability of photoexcited charge carriers [68]. Fig. 7 presents the PL spectra for pure Bi_2WO_6 as well as 2 wt% CQDs/Bi_2WO_6 hybrid materials. All the samples show strong emission peak centered at around 470 nm. For comparison, when CQDs was anchored on the Bi_2WO_6 surface, the intensity of this emission

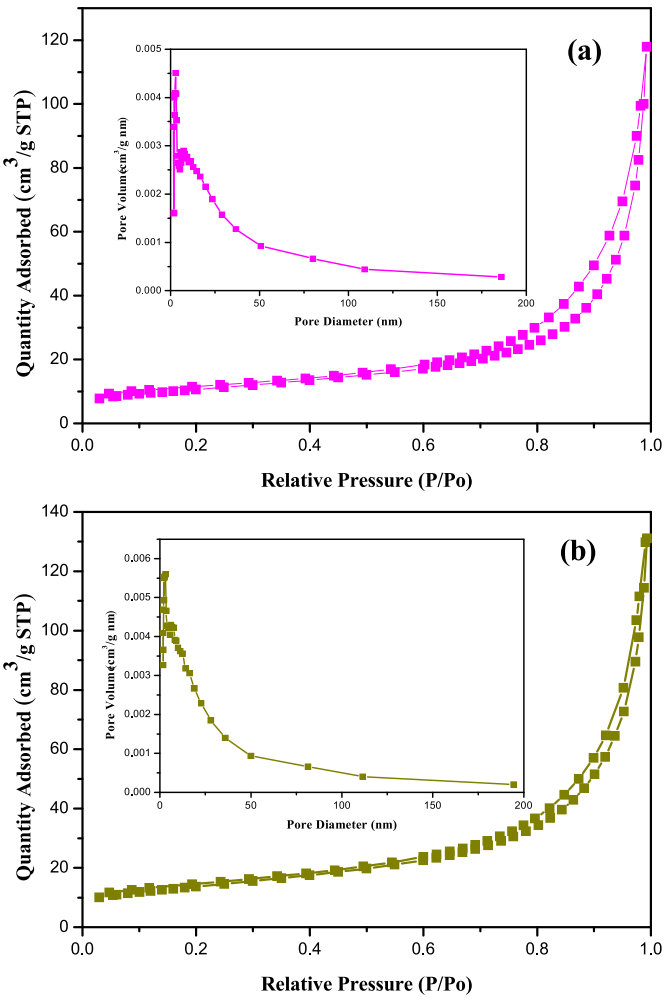

Fig. 5. Nitrogen absorption–desorption isotherms of (a) pure Bi_2WO_6 and (b) CQDs/Bi_2WO_6 hybrid materials.

band decreased significantly, which indicates efficient transfer of photoexcited electrons from Bi_2WO_6 to CQDs.

On the basis of the above experimental results, it is believed that the introduction of CQDs reduce the electrons and holes recombination rate, which favors the effective charge separation of Bi_2WO_6

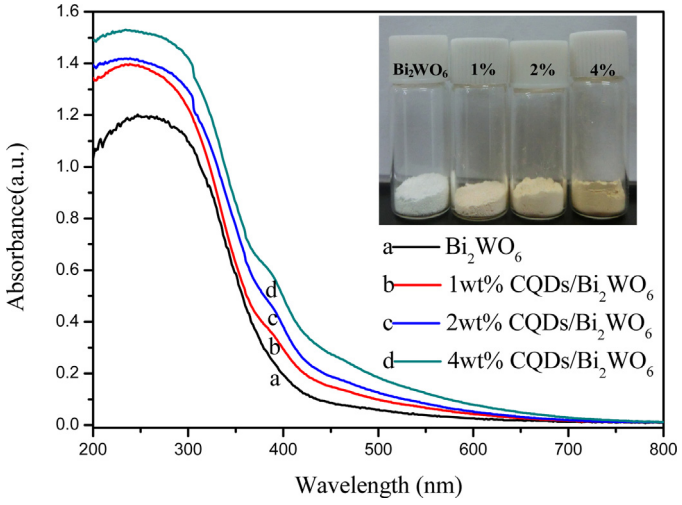

Fig. 6. (a) UV–vis diffuse reflectance spectra of the as-prepared CQDs/Bi_2WO_6 hybrid materials.

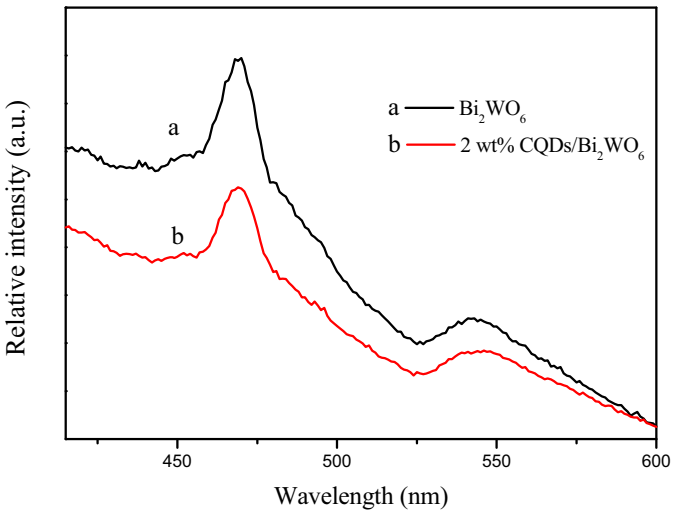

Fig. 7. PL spectra of pure Bi_2WO_6 and 2 wt% CQDs/Bi_2WO_6 hybrid materials.

and thus improve the photocatalytic activities. To further prove this assumption, photocurrents and EIS measurements are performed. Fig. 8 displays the photocurrent–time (I–t) curves of pure Bi_2WO_6 as well as 2 wt% CQDs/Bi_2WO_6 hybrid material electrodes. It can be observed from the working electrodes that photocurrent response sharply increases once the light irradiation is activated. The photocurrents are steady and reproducible during several intermittent on–off irradiation cycles. The 2 wt% CQDs/Bi_2WO_6 hybrid materials have higher photocurrent response than that of the pure Bi_2WO_6. It indicates that the CQDs/Bi_2WO_6 hybrid material has a higher separation rate of photoexcited electrons and holes under the irradiation of visible light. It could be attributed to the fact that the photogenerated electrons are excited from the VB to the CB and then transfer to CQDs, inhibiting the direct recombination of electrons and holes. This may due to the CQDs is considered to be a good electron-acceptor material due to the conjugated π structure and acted as the separation center of the photoexcited charge carriers [47,57].

Electrochemical impedance spectroscopy (EIS) of pure Bi_2WO_6 and 2 wt% CQDs/Bi_2WO_6 hybrid material samples is carried out to investigate the process of electron transfer, and the result is shown in Fig. 9. The radius of the arc on the EIS Nyquist plot reflects the charge transfer rate occurring at the contact interface between the

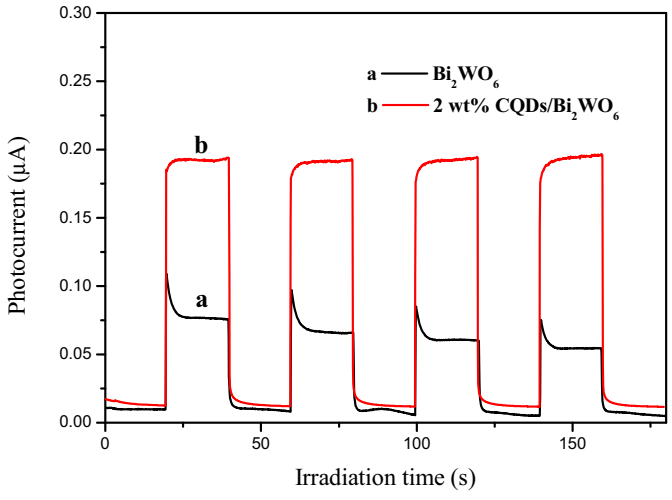

Fig. 8. Transient photocurrent response for pure Bi_2WO_6 and 2 wt% CQDs/Bi_2WO_6 hybrid materials.

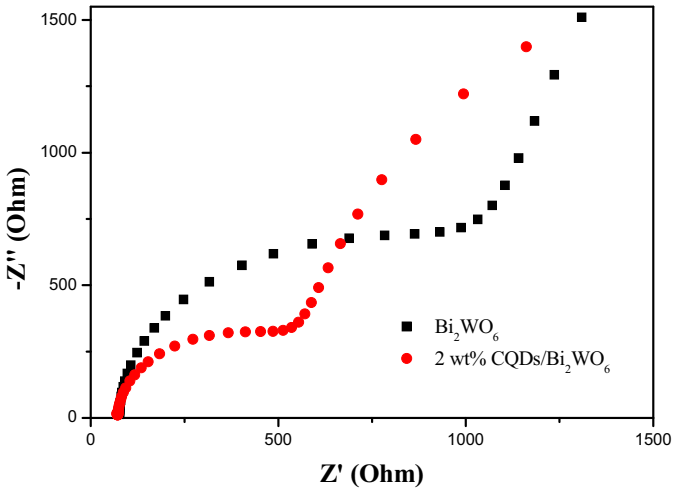

Fig. 9. Electrochemical impedance spectroscopy of pure Bi_2WO_6 and 2 wt% CQDs/Bi_2WO_6 hybrid materials.

working electrode and electrolyte solution. The smaller radius of the Nyquist circle represents the lower charge-transfer resistance [69]. As shown in Fig. 10, the arc radius on EIS Nyquist plot of 2 wt% CQDs/Bi_2WO_6 hybrid material sample is smaller than that of pure Bi_2WO_6 sample. It means that a faster interfacial charge transfer to the electron acceptor occurs and results in an effective separation of electron–hole pairs by the introduction of CQDs [70]. The characterization results of photocurrents and EIS measurements are consistent with the PL analysis, which confirm that the introduction of CQDs (electron acceptor) [54] is an effective way to improve photocatalytic efficiency.

3.4. Photocatalytic tests

The photocatalytic activity of as-prepared samples is first evaluated by the degradation of RhB. The adsorption analysis of the hybrids in the dark for the RhB has been provided (Fig. S5). The absorption–desorption balance have been achieved between the catalyst and dye for 30 min absorption process. It can be seen that 16.3%, 17.6%, 23.9% and 28.2% of RhB were respectively adsorbed by Bi_2WO_6, 1 wt% CQDs/Bi_2WO_6, 2 wt% CQDs/Bi_2WO_6, and 4 wt% CQDs/Bi_2WO_6 within 30 min, which should be attributed to their different adsorption capacity. Fig. 10a shows the photocatalytic activities of the CQDs/Bi_2WO_6 hybrid materials with different CQDs contents as well as pure Bi_2WO_6 under the irradiation of visible light. The blank test proves the RhB is only slightly degraded in the absence of catalysts, indicating that the photolysis of RhB can be ignored. It can be seen that the introduction of different contents of CQDs could enhance the photocatalytic performance of Bi_2WO_6. The 2 wt% CQDs/Bi_2WO_6 hybrid material shows the highest activity, which is much better than that for pure Bi_2WO_6, as well as the hybrid materials with other CQDs contents. At the same time, the photocatalytic degradation kinetics of RhB by using CQDs/Bi_2WO_6 hybrid materials were investigated, and the results were shown in Fig. 10b. The changes of the RhB concentration vs the irradiation time over the CQDs/Bi_2WO_6 hybrid materials according with the pseudo-first-order kinetics plot. The photocatalytic degradation rate was improved through the introduction of CQDs. The 2 wt% CQDs/Bi_2WO_6 hybrid material sample exhibit the highest degradation rate which is about 1.8 times higher than that of pure Bi_2WO_6 sample. The pseudo-first-order constants and relative coefficients are summarized in Table S1.

As a broad-spectrum antibiotic agent, ciprofloxacin (CIP) has been widely used for treating bacterial infections. The presence of

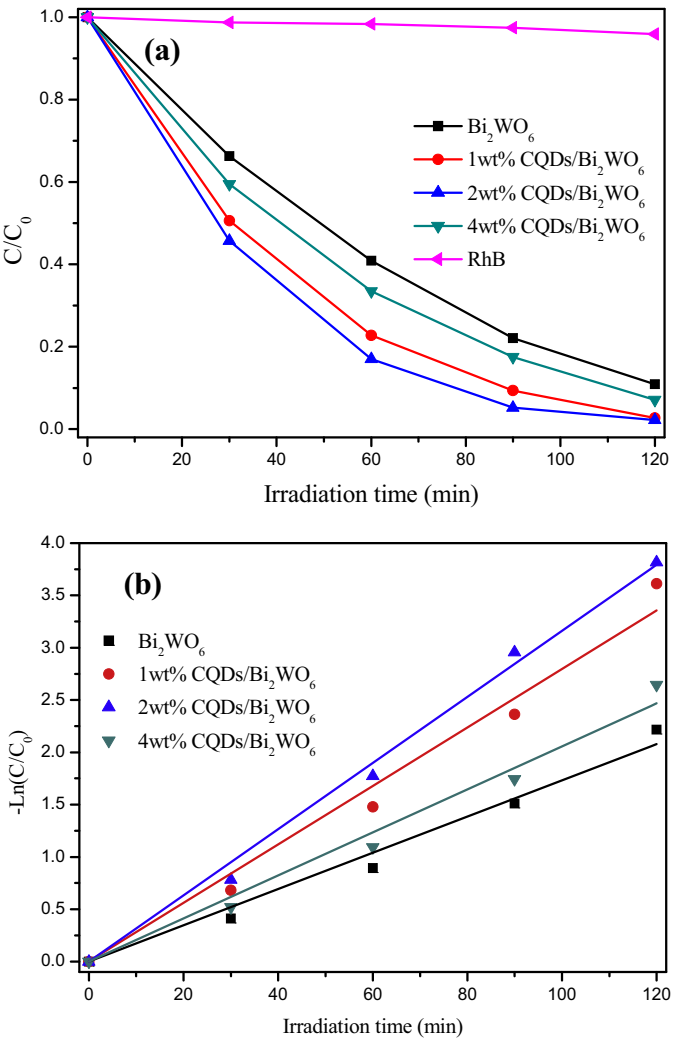

Fig. 10. (a) Photocatalytic degradation of RhB in the presence of pure Bi_2WO_6, CQDs/Bi_2WO_6 hybrid materials and photolysis of RhB under visible light irradiation and (b) kinetic fit for the degradation of RhB with the pure Bi_2WO_6, CQDs/Bi_2WO_6 hybrid materials.

CIP in natural environments generates several human health concerns. The toxicity tests reveals that it may cause various adverse effects on ecosystem by inducing proliferation of bacterial drug resistance [71]. Hence, it is of great important for the removal of CIP. CQDs/Bi_2WO_6 hybrid materials have been used to explore the CIP removing. It is the first time reported by using the Bi_2WO_6 based materials for the CIP photodegradation, and the results are shown in Fig. 11a. CIP is photodegraded slowly in the presence of pure Bi_2WO_6 under visible light. Only 30% CIP is photodegraded after irradiated for 30 min. However, the photocatalytic performance is significantly enhanced after the modification of CQDs, which indicates that the CQDs play an important role for the enhancement of CIP photodegradation. Among them, the 2 wt% CQDs/Bi_2WO_6 hybrid material exhibits the highest activity. After the irradiation for 30 min, 64% CIP can be photodegraded. And the removal efficiency could reach 87% when the irradiation time extended to 120 min. Fig. S3 shows the time-dependent absorption spectra of CIP solution in the presence of pure Bi_2WO_6 and 2 wt% CQDs/Bi_2WO_6 hybrid material, respectively. It can be seen that the 2 wt% CQDs/Bi_2WO_6 hybrid material shows the faster photodegradation rate of CIP than that of pure Bi_2WO_6.

Considering the possible broad-spectrum pollutants photodegradation for practical application, the photocatalytic activity

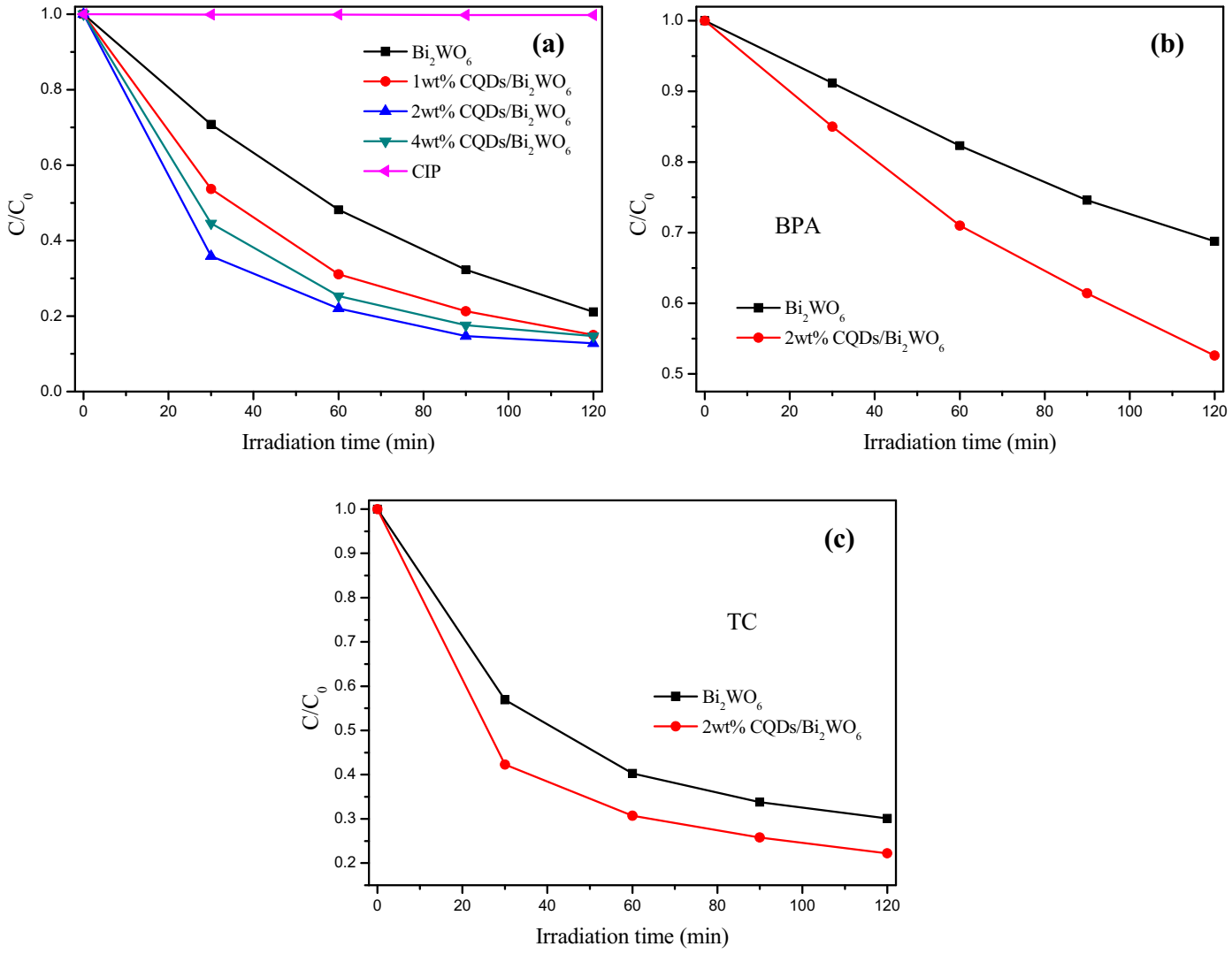

Fig. 11. Photocatalytic degradation of (a) CIP, (b) BPA and (c) TC in the presence of pure Bi_2WO_6, CQDs/Bi_2WO_6 hybrid materials under visible light irradiation.

of the as-prepared CQDs/Bi_2WO_6 hybrid materials are further evaluated via the photocatalytic degradation of two different types of pollutants, such as endocrine disrupting chemical BPA and antibiotic TC, under visible light irradiation, as shown in Fig. 11b and c. The results reveal that the CQDs/Bi_2WO_6 hybrid material exhibit much improved photocatalytic activity than that of pure Bi_2WO_6 for the BPA, and TC photodegradation. The detailed degradation process of BPA in the presence of pure Bi_2WO_6 and 2 wt% CQDs/Bi_2WO_6 hybrid material is shown in Fig. S4. These photocatalytic degradation results of four model organic pollutants imply that the introduction of CQDs is an effective way to improve photocatalytic efficiency and the CQDs/Bi_2WO_6 hybrid material is efficient visible-light-response photocatalyst.

The reusability and stability of the photocatalyst are vital to the practical application. To evaluate the reusability and stability of the CQDs/Bi_2WO_6 hybrid material, recycling reactions are performed for the photodegradation of RhB over 2 wt% CQDs/Bi_2WO_6 hybrid material under visible light irradiation. After five consecutive cycles, no apparent deactivation of the photocatalysts is observed, which implies the high stability of CQDs/Bi_2WO_6 hybrid material (Fig. 12). Furthermore, XRD analysis of the 2 wt% CQDs/Bi_2WO_6 hybrid material before and after the photocatalytic reactions is carried out, as shown in Fig. 13. The crystal structures of the sample

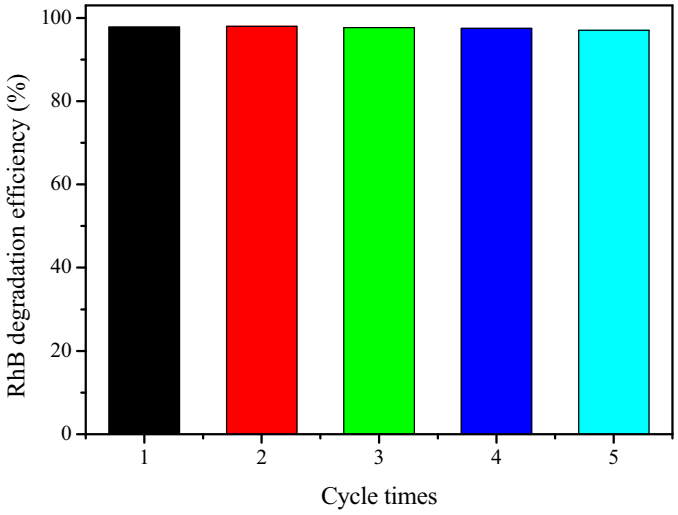

Fig. 12. Cycling runs for the photodegradation of RhB in the presence of 2 wt% CQDs/Bi_2WO_6 hybrid materials under visible light irradiation.

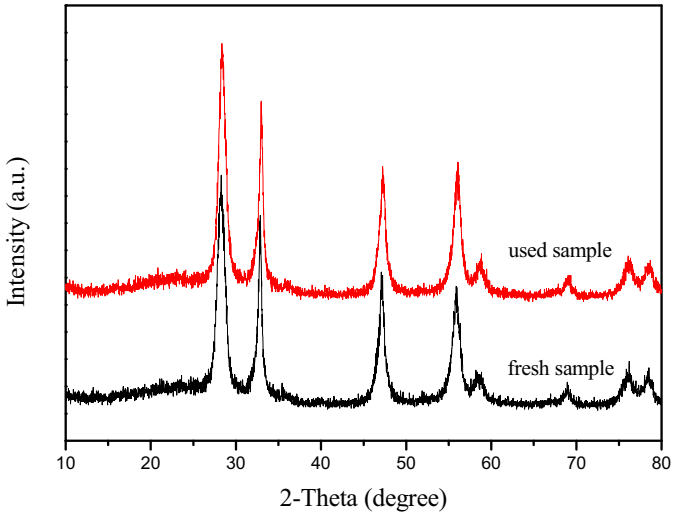

Fig. 13. XRD patterns of the 2 wt% CQDs/Bi_2WO_6 hybrid materials before and after the cycling photocatalytic experiments.

do not change after photocatalytic cycle, which clearly suggests that the CQDs/Bi_2WO_6 hybrid materials are stable during the photodegradation process.

3.5. Mechanism of pollutant photodegradation

The electron spin resonance (ESR) spin-trap technique is applied to reveal the reactive oxygen species on the photodegradation process during the irradiation of CQDs/Bi_2WO_6 hybrid materials with DMPO in water, and the results are shown in Fig. 14 [72]. The 2 wt% CQDs/Bi_2WO_6 hybrid materials suspension are irradiated for 8 min by a Quanta-Ray Nd:YAG pulsed laser system. When the light is on, the characteristic signals of the DMPO-superoxide radical ($O_2^{\bullet-}$) could be observed while the characteristic signals of the DMPO-hydroxyl radical ($^{\bullet}OH$) could not be seen. Therefore, it can be assumed that the $O_2^{\bullet-}$ radicals plays the important role in the photodegradation process and the $^{\bullet}OH$ is not the main reactive species.

In XPS, not only the information on the binding energy of a specific element can be obtained but also the total density of states (DOS) of the valence band (VB). The valence band edge of Bi_2WO_6 primarily derives from the hybridization of the O 2p and Bi 6s orbitals and the conduction band edge from the empty W5d orbitals [73]. The VB of 2 wt% CQDs/Bi_2WO_6 hybrid material is measured by XPS valence spectra [74], as shown in Fig. S6. The hybrid material shows a VB with the edge of the maximum energy at about 2.21 eV. According to the DRS analysis, the absorption edge is about 450 nm, and the corresponding band gap energy (E_g) is about 2.76 eV. Moreover, the conduction band (CB) edge potential can be acquired by the formula $E_{CB} = E_{VB} - E_g$. Thus, the CB minimum will occur at about −0.55 eV. The VB value (2.21 eV) is less positive than $E^0(^{\bullet}OH/OH^-)$ (2.38 eV vs NHE) [75], which implying that the OH^- cannot be oxidized to yield $^{\bullet}OH$ by the h_{VB}^+ of CQDs/Bi_2WO_6 hybrid material. However, the photo-generated electrons in the CB minimum (−0.55 eV) is enough to reduce O_2 to generate $O_2^{\bullet-}$ due to the $E^0(O_2/O_2^{\bullet-})$ is only about −0.046 eV [76]. The results of above mentioned and the ESR analysis are undifferentiated.

To further reveal the roles of the active oxygen species on the photocatalysis process over CQDs/Bi_2WO_6 hybrid materials, free radicals trapping experiments are performed (Fig. 15). When the t-butanol (a quencher of $^{\bullet}OH$) [77] is added, the photo-degradation of RhB by 2 wt% CQDs/Bi_2WO_6 hybrid material is not obvious affected, which imply that the $^{\bullet}OH$ is not the main reactive species.

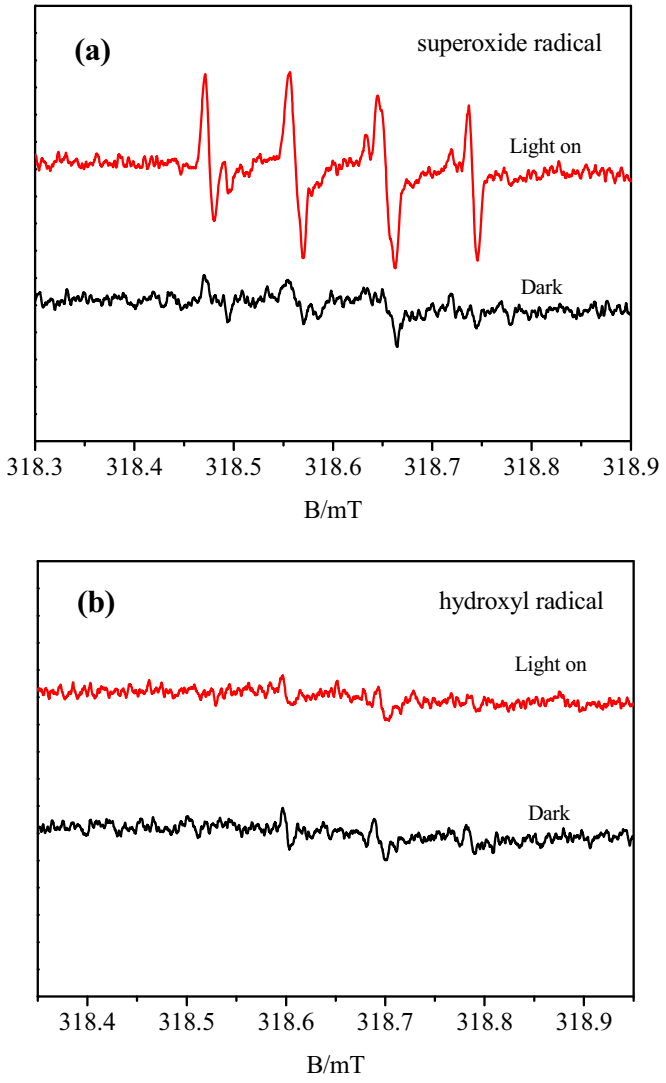

Fig. 14. ESR spectra of radical adducts trapped by DMPO in CQDs/Bi_2WO_6 hybrid materials aqueous dispersion under visible light irradiation.

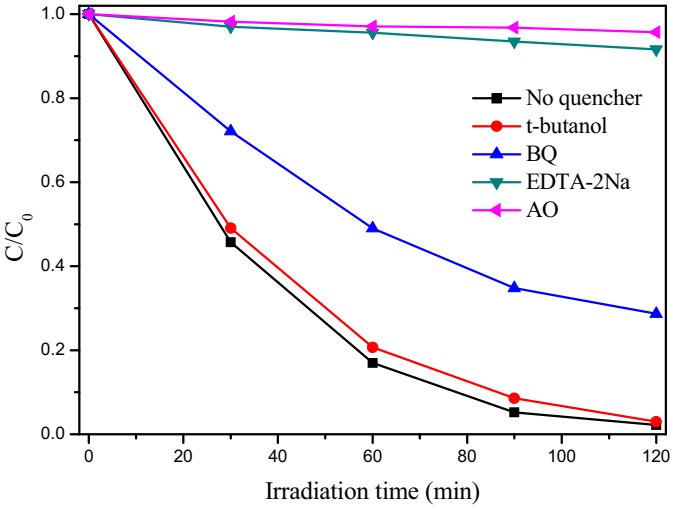

Fig. 15. Trapping experiment of active species during the photocatalytic degradation of RhB over CQDs/Bi_2WO_6 hybrid material under visible light irradiation.

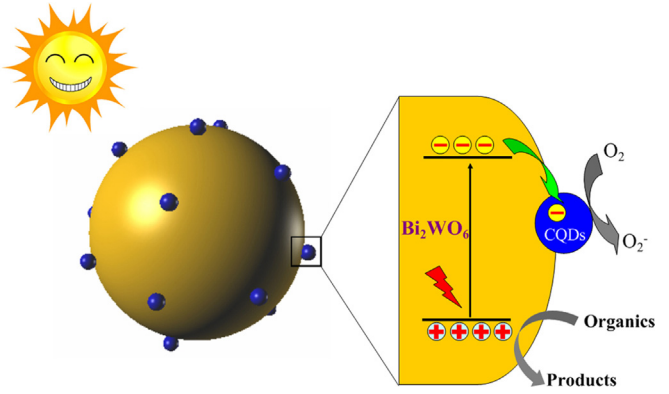

Fig. 16. Schematic of the separation and transfer of photogenerated charges in the CQDs/Bi_2WO_6 hybrid material combined with the possible reaction mechanism of photocatalytic procedure.

However, the photodegradation process could be inhibited efficiently when enzoquinone (BQ) is applied as $O_2^{\bullet-}$ scavenger. It reveals that the $O_2^{\bullet-}$ plays the important role in photocatalysis process, corresponding to the result of ESR analysis. When the EDTA-2Na (quencher of h^+) [78] is added, it can greatly inhibit the photocatalytic degradation of RhB, which indicates the h^+ also play the important role in the photocatalysis process. Another quencher of h^+ (AO) [77] is used to confirm this result. The activity is also remarkably decreased, which accord with the result of EDTA-2Na addition. The ESR analysis and free radicals trapping experiments indicate that the $O_2^{\bullet-}$ and h^+ are the main active species.

Based on the above experimental results, the photocatalytic mechanism diagram of CQDs/Bi_2WO_6 hybrid materials is presented in Fig. 16. When the Bi_2WO_6 is irradiated by visible light, the electrons can be excited from the VB to the CB, leaving the holes on the VB. Normally, these photo-generated electrons and holes quickly recombine and only a portion of charges could participate in the photocatalytic process. However, when Bi_2WO_6 is contact with CQDs to form hybrid materials, these photo-generated electrons on the CB of Bi_2WO_6 tend to transfer to CQDs. The delocalized conjugated structure of CQDs made it easier to transfer the photo-generated electrons, result in efficient electron–hole pair separation and thus an enhanced photocatalytic activity. It is consist with the result of the PL, photocurrent, and EIS analysis. The electron on the CQDs could combine with oxygen in the solution to form $O_2^{\bullet-}$. The generated $O_2^{\bullet-}$ and the hole on the VB of Bi_2WO_6 would play important role in the photodegradation process, leading to dramatic photocatalytic performance.

4. Conclusions

Novel CQDs/Bi_2WO_6 hybrid materials have been prepared for the first time through a facile hydrothermal process. The CQDs were dispersed on the surface of sphere-like Bi_2WO_6 and tight junctions were formed. After the introduction of CQDs, the photocatalytic activities of Bi_2WO_6 on RhB, CIP, BPA and TC degradation under visible light irradiation increased dramatically. The 2 wt% CQDs/Bi_2WO_6 hybrid material exhibited the optimal photocatalytic performance. In addition, the CQDs/Bi_2WO_6 hybrid material showed excellent reusability and stability, which was valuable for the potential applications of environmental protection. The significant enhancement of photocatalytic activity was ascribed to the improved charge separation efficiency which caused by CQDs. The $O_2^{\bullet-}$ and h^+ were the main active species during the photocatalysis process. This work can provide important inspirations in developing other CQDs-based photocatalytic hybrid materials.

Acknowledgements

This work was financially supported by the National Nature Science Foundation of China (Nos. 21206060, 21471069 and 21177050) and the Special Financial Grant from the China Postdoctoral Science Foundation (2013T60506).

Appendix A. Supplementary data

Supplementary data associated with this article can be found, in the online version, at http://dx.doi.org/10.1016/j.apcatb.2014.11.057.

References

[1] A. Kubacka, M. Fernandez-García, G. Colon, Chem. Rev. 112 (2012) 1555–1614.
[2] Z.G. Zou, J.H. Ye, K. Sayama, H. Arakawa, Nature 414 (2001) 625–627.
[3] R. Asahi, T. Morikawa, T. Ohwaki, K. Aoki, Y. Taga, Science 293 (2001) 269–271.
[4] R.G. Li, F.X. Zhang, D.G. Wang, J.X. Yang, M.R. Li, J. Zhu, X. Zhou, H.X. Han, C. Li, Nat. Commun. 4 (2013) 1432.
[5] X.C. Wang, K. Maeda, A. Thomas, K. Takanabe, G. Xin, J.M. Carlsson, K. Domen, M. Antonietti, Nat. Mater. 8 (2009) 76–80.
[6] J.X. Xia, S. Yin, H.M. Li, H. Xu, L. Xu, Y.G. Xu, Dalton Trans. 40 (2011) 5249–5258.
[7] J.X. Xia, S. Yin, H.M. Li, H. Xu, Y.S. Yan, Q. Zhang, Langmuir 27 (2011) 1200–1206.
[8] Z.G. Yi, J.H. Ye, N. Kikugawa, T. Kako, S.X. Ouyang, H. Stuart-Williams, H. Yang, J.Y. Cao, W.J. Luo, Z.S. Li, Y. Liu, R.L. Withers, Nat. Mater. 9 (2010) 559–564.
[9] H. Tong, S.X. Ouyang, Y.P. Bi, N. Umezawa, M. Oshikiri, J.H. Ye, Adv. Mater. 24 (2012) 229–251.
[10] C. Zhang, Y.F. Zhu, Chem. Mater. 17 (2005) 3537–3545.
[11] S. Mahanty, J. Ghose, Mater. Lett. 11 (1991) 254–256.
[12] G.K. Zhang, F. Lü, M. Li, J.L. Yang, X.Y. Zhang, B.B. Huang, J. Phys. Chem. Solids 71 (2010) 579–582.
[13] L.S. Zhang, W.Z. Wang, Z.G. Chen, L. Zhou, H.L. Xu, W. Zhu, J. Mater. Chem. 17 (2007) 2526–2532.
[14] L.S. Zhang, W.Z. Wang, L. Zhou, H.L. Xu, Small 3 (2007) 1618–1625.
[15] M. Shang, W.Z. Wang, S.M. Sun, L. Zhou, L. Zhang, J. Phys. Chem. C 112 (2008) 10407–10411.
[16] C.X. Xu, X. Wei, Z.H. Ren, Y. Wang, G. Xu, G. Shen, G.R. Han, Mater. Lett. 63 (2009) 2194–2197.
[17] S.M. Sun, W.Z. Wang, J.H. Xu, L. Wang, Z.J. Zhang, Appl. Catal. B 106 (2011) 559–564.
[18] S.M. Sun, W.Z. Wang, L. Zhang, J. Mater. Chem. 22 (2012) 19244–19249.
[19] Y.Y. Li, J.P. Liu, X.T. Huang, J.G. Yu, Dalton Trans. 39 (2010) 3420–3425.
[20] R. Shi, G.L. Huang, J. Lin, Y.F. Zhu, J. Phys. Chem. C 113 (2009) 19633–19638.
[21] Z.J. Zhang, W.Z. Wang, W.Z. Yin, M. Shang, L. Wang, S.M. Sun, Appl. Catal. B 101 (2010) 68–73.
[22] Z.J. Zhang, W.Z. Wang, E.P. Gao, M. Shang, J.H. Xu, J. Hazard. Mater. 196 (2011) 255–262.
[23] D.J. Wang, G.L. Xue, Y.Z. Zhen, F. Fu, D.S. Li, J. Mater. Chem. 22 (2012) 4751–4758.
[24] X. Ding, K. Zhao, L.Z. Zhang, Environ. Sci. Technol. 48 (2014) 5823–5831.
[25] Z.H. Sun, J.J. Guo, S.M. Zhu, L. Mao, J. Ma, D. Zhang, Nanoscale 6 (2014) 2186–2193.
[26] H.W. Ma, J.F. Shen, M. Shi, X. Lu, Z.Q. Li, Y. Long, N. Li, M.X. Ye, Appl. Catal. B 121 (2012) 198–205.
[27] S.M. Sun, W.Z. Wang, L. Zhang, J. Phys. Chem. C 117 (2013) 9113–9120.
[28] S.B. Zhu, T.G. Xu, H.B. Fu, J.C. Zhao, Y.F. Zhu, Environ. Sci. Technol. 41 (2007) 6234–6239.
[29] Z.J. Zhang, W.Z. Wang, L. Zhang, Dalton Trans. 42 (2013) 4579–4585.
[30] J. Tian, Y.H. Sang, G.W. Yu, H.D. Jiang, X.N. Mu, H. Liu, Adv. Mater. 25 (2013) 5075–5080.
[31] G. Colón, S. Murcia López, M.C. Hidalgo, J.A. Navío, Chem. Commun. 46 (2010) 4809–4811.
[32] J.H. Xu, W.Z. Wang, S.M. Sun, L. Wang, Appl. Catal. B 111 (2012) 126–132.
[33] Q.C. Xu, D.V. Wellia, Y.H. Ng, R. Amal, T.T.Y. Tan, J. Phys. Chem. C 115 (2011) 7419–7428.
[34] Y. Peng, M. Yan, Q.G. Chen, C.M. Fan, H.Y. Zhou, A.W. Xu, J. Mater. Chem. A 2 (2014) 8517–8524.
[35] Z.J. Zhang, W.Z. Wang, L. Wang, S.M. Sun, ACS Appl. Mater. Interfaces 4 (2012) 593–597.
[36] Y.L. Li, Y.M. Liu, J.S. Wang, E. Uchaker, Q.F. Zhang, S.B. Sun, Y.X. Huang, J.Y. Li, G.Z. Cao, J. Mater. Chem. A 1 (2013) 7949–7956.
[37] L. Ge, C.C. Han, J. Liu, Appl. Catal. B 108 (2011) 100–107.
[38] Y.L. Tian, B.B. Chang, J.L. Lu, J. Fu, F.N. Xi, X.P. Dong, ACS Appl. Mater. Interfaces 5 (2013) 7079–7085.
[39] H.G. Yu, R. Liu, X.F. Wang, P. Wang, J.G. Yu, Appl. Catal. B 111 (2012) 326–333.
[40] S.M. Sun, W.Z. Wang, L. Zhang, J.H. Xu, Appl. Catal. B 125 (2012) 144–148.
[41] D.Q. He, L.L. Wang, D.D. Xu, J.L. Zhai, D.J. Wang, T.F. Xie, ACS Appl. Mater. Interfaces 3 (2011) 3167–3171.
[42] P. Ju, P. Wang, B. Li, H. Fan, S.Y. Ai, D. Zhang, Y. Wang, Chem. Eng. J. 236 (2014) 430–437.

[43] A.L.M. Reddy, S.R. Gowda, M.M. Shaijumon, P.M. Ajayan, Adv. Mater. 24 (2012) 5045–5064.
[44] S.Y. Lim, W. Shen, Z.Q. Gao, Chem. Soc. Rev. 44 (2015) 362–381.
[45] S.N. Baker, G.A. Baker, Angew. Chem., Int. Ed. 49 (2010) 6726–6744.
[46] J.H. Shen, Y.H. Zhu, X.L. Yang, C.Z. Li, Chem. Commun. 48 (2012) 3686–3699.
[47] H.T. Li, Z.H. Kang, Y. Liu, S.T. Lee, J. Mater. Chem. 22 (2012) 24230–24253.
[48] W.L. Wei, C. Xu, J.S. Ren, B.L. Xu, X.G. Qu, Chem. Commun. 48 (2012) 1284–1286.
[49] L. Zhou, Y.H. Lin, Z.Z. Huang, J.S. Ren, X.G. Qu, Chem. Commun. 48 (2012) 1147–1149.
[50] S.T. Yang, L. Cao, P.G.J. Luo, F.S. Lu, X. Wang, H.F. Wang, M.J. Meziani, Y.F. Liu, G. Qi, Y.P. Sun, J. Am. Chem. Soc. 131 (2009) 11308–11309.
[51] L. Cao, X. Wang, M.J. Meziani, F. Lu, H.F. Wang, P.G. Luo, Y. Lin, B.A. Harruff, L.M. Veca, D. Murray, S.Y. Xie, Y.P. Sun, J. Am. Chem. Soc. 129 (2007) 11318–11319.
[52] R.H. Liu, H. Huang, H.T. Li, Y. Liu, J. Zhong, Y.Y. Li, S. Zhang, Z.H. Kang, ACS Catal. 4 (2014) 328–336.
[53] D.L. Son, B.W. Kwon, D.H. Park, W.S. Seo, Y. Yi, B. Angadi, C.L. Lee, W.K. Choi, Nat. Nanotechnol. 7 (2012) 465–471.
[54] Y. Li, Y. Hu, Y. Zhao, G.Q. Shi, L.E. Deng, Y.B. Hou, L.T. Qu, Adv. Mater. 23 (2011) 776–780.
[55] H.T. Li, X.D. He, Z.H. Kang, H. Huang, Y. Liu, J.L. Liu, S.Y. Lian, C.H.A. Tsang, X.B. Yang, S.T. Lee, Angew. Chem., Int. Ed. 49 (2010) 4430–4434.
[56] X. Zhang, F. Wang, H. Huang, H.T. Li, X. Han, Y. Liu, Z.H. Kang, Nanoscale 5 (2013) 2274–2278.
[57] H.J. Yu, Y.F. Zhao, C. Zhou, L. Shang, Y. Peng, Y.H. Cao, L.Z. Wu, C.H. Tung, T.R. Zhang, J. Mater. Chem. A 2 (2014) 3344–3351.
[58] H.T. Li, R.H. Liu, Y. Liu, H. Huang, H. Yu, H. Ming, S.Y. Lian, S.T. Lee, Z.H. Kang, J. Mater. Chem. 22 (2012) 17470–17475.
[59] B.Y. Yu, S.Y. Kwak, J. Mater. Chem. 22 (2012) 8345–8353.
[60] H.C. Zhang, H. Ming, S.Y. Lian, H. Huang, H.T. Li, L.L. Zhang, Y. Liu, Z.H. Kang, S.T. Lee, Dalton Trans. 40 (2011) 10822–10825.
[61] H.C. Zhang, H. Huang, H. Ming, H.T. Li, L.L. Zhang, Y. Liu, Z.H. Kang, J. Mater. Chem. 22 (2012) 10501–10506.
[62] H. Yu, H.C. Zhang, H. Huang, Y. Liu, H.T. Li, H. Ming, Z.H. Kang, New J. Chem. 36 (2012) 1031–1035.
[63] D. Tang, H.C. Zhang, H. Huang, R.H. Liu, Y.Z. Han, Y. Liu, C.Y. Tong, Z.H. Kang, Dalton Trans. 42 (2013) 6285–6289.
[64] S.J. Zhu, Q.N. Meng, L. Wang, J.H. Zhang, Y.B. Song, H. Jin, K. Zhang, H.C. Sun, H.Y. Wang, B. Yang, Angew. Chem., Int. Ed. 52 (2013) 3953–3957.
[65] X.M. Tu, S.L. Luo, G.X. Chen, J.H. Li, Chem. Eur. J. 18 (2012) 14359–14366.
[66] J.Z. Li, N.Y. Wang, T.T. Tran, C.A. Huang, L. Chen, L.J. Yuan, L.P. Zhou, R. Shen, Q.Y. Cai, Analyst 138 (2013) 2038–2043.
[67] J. Di, J.X. Xia, S. Yin, H. Xu, M.Q. He, H.M. Li, L. Xu, Y.P. Jiang, RSC Adv. 3 (2013) 19624–19631.
[68] H. Xu, J. Yan, Y.G. Xu, Y.H. Song, H.M. Li, J.X. Xia, C.J. Huang, H.L. Wan, Appl. Catal. B 129 (2013) 182–193.
[69] J. Di, J.X. Xia, S. Yin, H. Xu, L. Xu, Y.G. Xu, M.Q. He, H.M. Li, J. Mater. Chem. A 2 (2014) 5340–5351.
[70] Y.R. Zhu, X.B. Ji, C.C. Pan, Q.Q. Sun, W.X. Song, L.B. Fang, Q.Y. Chen, C.E. Banks, Energy Environ. Sci. 6 (2013) 3665–3675.
[71] T. Paul, P.L. Miller, T.J. Strathmann, Environ. Sci. Technol. 41 (2007) 4720–4727.
[72] Y.H. Lv, Y.Y. Zhu, Y.F. Zhu, J. Phys. Chem. C 117 (2013) 18520–18528.
[73] N. Zhang, R. Ciriminna, M. Pagliaro, Y.J. Xu, Chem. Soc. Rev. 43 (2014) 5276–5287.
[74] M.L. Guan, C. Xiao, J. Zhang, S.J. Fan, R. An, Q.M. Cheng, J.F. Xie, M. Zhou, B.J. Ye, Y. Xie, J. Am. Chem. Soc. 135 (2013) 10411–10417.
[75] H.F. Cheng, B.B. Huang, Y. Dai, X.Y. Qin, X.Y. Zhang, Langmuir 26 (2010) 6618–6624.
[76] L.Q. Ye, J.N. Chen, L.H. Tian, J.Y. Liu, T.Y. Peng, K.J. Deng, L. Zan, Appl. Catal. B 130–131 (2013) 1–7.
[77] J. Di, J.X. Xia, Y.P. Ge, L. Xu, H. Xu, M.Q. He, Q. Zhang, H.M. Li, J. Mater. Chem. A 2 (2014) 15864–15874.
[78] X.J. Bai, L. Wang, Y.J. Wang, W.Q. Yao, Y.F. Zhu, Appl. Catal. B 152–153 (2014) 262–270.